



The Physicomechanical Behavior and Microstructure of Air-Entrained 3D Printable Concrete

Yeşim Tarhan¹ and Remzi Şahin²

Abstract: The effects of air-entraining admixture (AEA), curing process, and core direction were studied as parameters in terms of their effect on the physicomechanical properties of 3D printed concrete. Four different AEA dosages (0%, 0.1%, 0.15%, and 0.2% by dosage of binder) were used to prepare the mixtures used for 3D printing. The influence of anisotropy on the printed concrete was studied by testing the cores drilled from the horizontal and vertical directions of the 3D concretes. The study also examines the efficiency of a specific spray-deposited chemical curing technique for improving the strength characteristics of 3D concrete. The addition of AEA reduced the unit weight significantly, thereby making the concrete ideal for lightweight structural members. Ultrasonic pulse velocity (UPV) testing on 3D printed samples showed that voids and air entrainment during the deposition process reduced the wave velocities. The ultrasonic wave velocity of cores drilled parallel to the printing direction was found to be slightly higher than cores perpendicular to the printing direction. However, the observation from the nondestructive tests did not agree with the compressive strength studies. The compressive strength of the cores drilled perpendicular to the direction of printing was higher than those drilled parallel, which can be due to the layers formed in the concrete during the filament deposition process. The 3D printing process reduced the compressive strength and induced anisotropy. The compressive strengths were reduced with air entrainment in the sample that was not 3D-printed. However, in the 3D-printed samples, 0.1% of AEA increased the vertical and horizontal strength compared to the samples without AEA. AEA in small quantities was found to be capable of improving the rheology of the mix and reducing the possible defects during the printing process, which resulted in better interlayer bonding. The durability aspect of air entrainment was studied using capillary water absorption, and it was found that the capillary water absorption increased with the addition of AEA. Microstructural studies using the Brunauer–Emmett–Teller (BET), Mercury Intrusion Porosimetry (MIP) and Scanning Electron Microscopy (SEM) on the 3D concrete revealed that the volume and size of the pores in the hardened matrix increased with the addition of AEA. The mechanical and durability studies showed that the optimal percentage of AEA is 0.1%. DOI: 10.1061/JMCEE7.MTENG-16224. © 2023 American Society of Civil Engineers.

Author keywords: 3D concrete; Air-entraining admixture (AEA); Core; Pore size distribution.

Introduction

3D concrete production, an environmentally friendly alternative to traditional techniques (Hager et al. 2016), presents reduced construction time, cost, and labor and provides opportunities to produce structures with complex geometry through layer-by-layer additive manufacturing methods (Wolfs 2015; Wu et al. 2016; Tarhan and Şahin 2019). However, there are some critical concerns with this new method, including the complexity of the material mix, the need to carefully select materials, the lack of standards, and the quality of the interfacial connection between layers.

One of the main challenges of 3D concrete is the weak interlayer bonding between layers, resulting in reduced mechanical efficacy. During 3D production, a period called a “time-gap” (Tay et al. 2019) or “interlayer interval time” (Wolfs et al. 2019) is required before pouring a second concrete layer over or next to the first layer. This time period depends on the speed of the nozzle employed and the

size of a single layer. The layered structure and the time gap cause a weak bond between the two layers (Tay et al. 2019; Paul et al. 2018), similar to a cold joint in conventional concrete. Nerella et al. (2019) also found that the reduction in strength was almost 90% over one day. SEM micrographs show an increasing interface between layers for larger interval times (Wolfs et al. 2019).

In studies that have examined the anisotropic behavior of 3D concrete, it was stated that different loading directions is one of the other most critical problems with 3D concrete construction (Feng et al. 2015; Panda et al. 2017; Sanjanyan et al. 2018; Ingaglio et al. 2019; Ma et al. 2019). Xiao et al. (2022) also reviewed papers investigating the anisotropic behavior of 3D concretes and reported that the studies produced conflicting results about the concrete’s mechanical strength. Ma et al. (2019) also stated that the compressive strength of samples formed by cutting varies depending on the direction. They determined that the compressive strengths of the cut samples were close to those of samples produced traditionally in a mold. Nerella et al. (2019) investigated the interfaces between layers in 3D printed elements and stated that the samples’ flexural and compressive strengths differed depending on the interface microstructure. Wolfs et al. (2019) presented the results of an experimental study on the relationship between the printing process parameters and the adhesion strength of 3D concrete. Investigating the effects of three process parameters (interlayer spacing time, nozzle height, and surface dehydration) on the compressive and tensile strength of 3D concrete, they concluded that 3D printed layer orientation is an effective parameter for strength tests. Research to determine direction-related changes in the properties of 3D concrete is

¹Assistant Professor, Technical Sciences Vocational School, Ardahan Univ., Ardahan 75000, Turkey (corresponding author). ORCID: <https://orcid.org/0000-0002-3901-9070>. Email: yesimtarhan@ardahan.edu.tr

²Professor, Dept. of Civil Engineering, Atatürk Univ., Erzurum 25030, Turkey. ORCID: <https://orcid.org/0000-0001-5400-7732>. Email: rsahin@atauni.edu.tr

Note. This manuscript was submitted on January 4, 2023; approved on May 30, 2023; published online on October 18, 2023. Discussion period open until March 18, 2024; separate discussions must be submitted for individual papers. This paper is part of the *Journal of Materials in Civil Engineering*, © ASCE, ISSN 0899-1561.

essential, contributing to a better understanding of the actual behavior of the concrete and helping to explain conflicting results in the literature.

In the construction sector, before the concrete is cast, in order to understand whether the concrete is produced at the desired strength, cube or cylinder concrete samples are taken from the fresh concrete, and a compressive strength test is performed. In a building or element with ongoing service life, core samples are taken from the hardened concrete element to evaluate the performance of the concrete in situ. The core samples indicate the mechanical strength of the concrete and give an idea of the composition and void structure of the concrete. Therefore, in this study for the first time, core samples were taken from hardened 3D concrete elements to analyze mechanical strength and durability performance, as in the construction industry. The different directional cores were taken from the 3D concrete slabs, and the anisotropic properties of the 3D concrete were investigated with the tests performed on these core samples. The aim is to provide more data, such as proper core orientation, to prepare better technical requirements and standards regarding 3D concrete structures. Many studies in the literature (Wolfs et al. 2019; Zhang et al. 2019; Kloft et al. 2020; Arunothayan et al. 2021; Xiao et al. 2022) have investigated small samples of 3D concrete cut from large pieces.

A further issue with 3D concrete production is the loss of surface moisture due to evaporation during the time gap after extrusion, leading to the most prominent mechanism for weak bond strength in concrete (Wolfs et al. 2019; Nerella et al. 2019; Sanjayan et al. 2018; Keita et al. 2019; Van der Putten et al. 2019). In addition, air pockets were formed with the loss of surface moisture, which fills up with water due to capillary absorption after the placement of the next layer (Moelich et al. 2021; Kruger and van Zijl 2021). Thus, the compressive, flexural, and tensile (or interlayer bond) strengths of the 3D concrete were reduced significantly compared to conventional methods (Kloft et al. 2020; Kruger et al. 2021). On the other hand, there is a lack of studies investigating the effects of additional air pockets with the addition of an AEA on the mechanical properties and bond strength between layers of 3D concrete. The effects of AEA on the fresh properties (rheology, viscosity, workability, etc.) of 3D concrete have been discussed only generally in previous studies (Lu et al. 2019; Assaad et al. 2020; Eugenin et al. 2022; Lu et al. 2021).

The main objective of this study, whose initial findings were published in Tarhan and Sahin (2021), is to comprehensively investigate the physicochemical properties of 3D concrete containing AEA using hardened concrete experiments. The gap in the literature on how AEA affects the interlayer bond weakness of 3D concretes, and the anisotropic nature of 3D concrete is addressed. Another aim

of this study is to investigate the curing method suitable for 3D concretes. Unlike traditional concrete applications with low water loss in the early stages due to molds, 3D concrete elements/structures require more curing, especially due to the high cement dosages and fine particle size distribution. 3D-printed concrete samples were cured in a laboratory environment (at $23^{\circ}\text{C} \pm 2^{\circ}\text{C}$ and 58%–60% humidity), at room temperature, and underwater curing conditions by Lu et al. (2019), Tay et al. (2019), Soltan and Li (2018), Zhang et al. (2019), and Panda et al. (2019). In addition, Nematullahi et al. (2018) applied hot air curing at 60°C for 24 h to 3D-printed geopolymer concrete samples. Despite the abovementioned studies, no research suggests the most suitable and practical curing regime for 3D concrete. The specific aspect of water loss in additive manufacturing has not been adequately investigated (Marchon et al. 2018). Since the 3D elements/structures are built as a whole, it is thought that curing with irrigation will be very difficult and insufficient as in the traditional method. In this study, different from the literature, the effect of a membrane-forming curing compound method was investigated for 3D concrete to provide better technical benefits.

In this study, to assess the anisotropic properties of 3D concretes with AEA and cured with curing compound, compressive strength, ultrasonic pulse velocity (UPV), and capillary water absorption tests were carried out on core samples taken perpendicular to and along the axial direction of the printing. MIP and BET techniques examined the pore size distribution of all accessible voids, and SEM analyses were performed to observe the pore morphology.

Experimental Methodology

Materials

CEM I 52.5 R (super white cement) with a density of 680 kg/m^3 , quartz sand of 0–0.5 mm and 0–1 mm classes, ground blast furnace slag (GGBFS) at a rate of 20% by weight, high purity calcined kaolin clay with 0.3% of the binder amount, various chemical additives in different proportions [viscosity modifying agent (0.1%), superplasticizer (1%), hydration stopper (0.3%), consistency modifier (0.5%), setting accelerator (1%) and set retarder (0.3%)], polypropylene fibers at a ratio of 0.2% of total volume, and air-entraining additive (AEA) were used in the mixtures. The water/binder and aggregate/cement mixture ratios were 0.35 and 1.5, respectively.

3D elements were produced using a 3D concrete printer in Istanbul Concrete Elements and Ready-Mixed Concrete Factories (ISTON/Istanbul/TR). Samples in the form of plates ($600 \times 600 \times 150 \text{ mm}$) were produced by printing 3D concrete strips of 50 mm by 25 mm, one on top of the other and side by side (see Fig. 1).

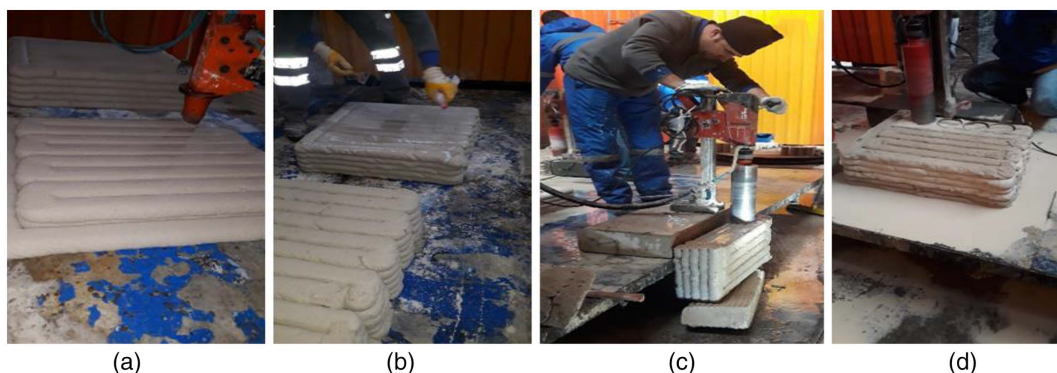


Fig. 1. 3D concrete samples: (a) production; (b) curing; (c) and (d) coring along and perpendicular to the axial direction of the casting, respectively.

Cores were taken from the plates at the end of the 28th day, and experiments were carried out on these samples.

Parameters and Coding

The current experiment program was designed considering the AEA ratio, curing condition, and core direction of the 3D concretes.

AEA ratios were determined according to the lower limit specified in the datasheet of the additive, considering that excessively entrained-air space would decrease the compressive strength of the concrete and increase flowability (Şahin et al. 2007). To ensure a controlled dosage, AEA was added at four different ratios, including 0%, 0.1%, 0.15%, and 0.2% of the cement dosage, which corresponded to 0, 0.0029, 0.0043, and 0.0057 g/L of water dosage, respectively. For 28 days, one of the two 3D printed samples from each mix recipe was kept in the laboratory (approx. $22^{\circ}\text{C} \pm 2^{\circ}\text{C}$, $60\% \pm 5\%$ humidity) without any curing, while the other was coated with an acrylic emulsion-based membrane-forming curing compound (commercially available as MasterKure 220 WB).

Since this study was built on the hypothesis of the heterogeneity of the void structure of 3D concrete elements, the coring direction was also determined as a parameter. Cylindrical cores of 100 mm in length and 100 mm in diameter were drilled from 3D concrete elements according to the TS EN 13791 (TS 2019a). The schematic representation of the locations and directions of the cores extracted from the 3D concrete is given in Fig. 2.

As can be seen in Fig. 2, the core samples drilled from the 3D concrete elements were precisely compatible with the schematic representation designed before the core drilling.

The terminology of samples: A0, A1, A1.5, and A2 indicated mixtures containing 0%, 0.1%, 0.15%, and 0.2% AEA, respectively. The letter “K” indicated samples cured with the membrane-type compound. Cores taken parallel to the direction of movement

of the nozzle (i.e., along the axial direction of the printing) were marked with an “H”. Last, cores taken vertically (i.e., perpendicular to the axial direction of the printing) were marked with a “V”. For example, A0KV denotes a cured core without air-entraining additives and has been drilled perpendicular to the printing direction. Testing was performed on 16 distinct sample groups in total. These were A0V, A0VK, A0H, A0HK, A1V, A1VK, A1H, A1HK, A1.5V, A1.5VK, A1.5H, A1.5HK, A2V, A2VK, A2H, and A2HK.

Detailed information about the material properties, proportions of concrete components, mix design, experimental procedure of preparation of the samples, fresh concrete tests (consistency, unit weight, rheology, and air content), and tests for critical characteristics of 3D concrete done in the study was provided in Tarhan and Şahin (2021).

Test Procedures

The unit weight in both the fresh and hardened state (on 3D printed concrete core samples), compressive strength, ultrasonic pulse velocity (UPV), and capillary water absorption tests were performed in the study.

UPV experiments, nondestructive test methods used to evaluate the quality and properties of 3D concretes, including density, durability, and overall condition, were conducted using an ultrasonic wave velocity tester (Proceq, Screening Eagle Technologies, Switzerland) based on the TS EN 12504-4 (TS 2021). Compressive strength tests were performed according to TS EN 12390-3 (TS 2019b). Cylindrical 3D concrete cores with dimensions of $\text{Ø}10 \times 10$ cm were left to dry in the open air for one day in the laboratory at $20^{\circ}\text{C} \pm 1^{\circ}\text{C}$ and $60\% \pm 5\%$ RH, and then the cores were capped with sulfur. After the samples were left to harden for at least two hours, a press with a capacity of 3,000 kN was used to measure the compressive strength. The loading rate was constant for all experiments at 0.4 MPa/s.

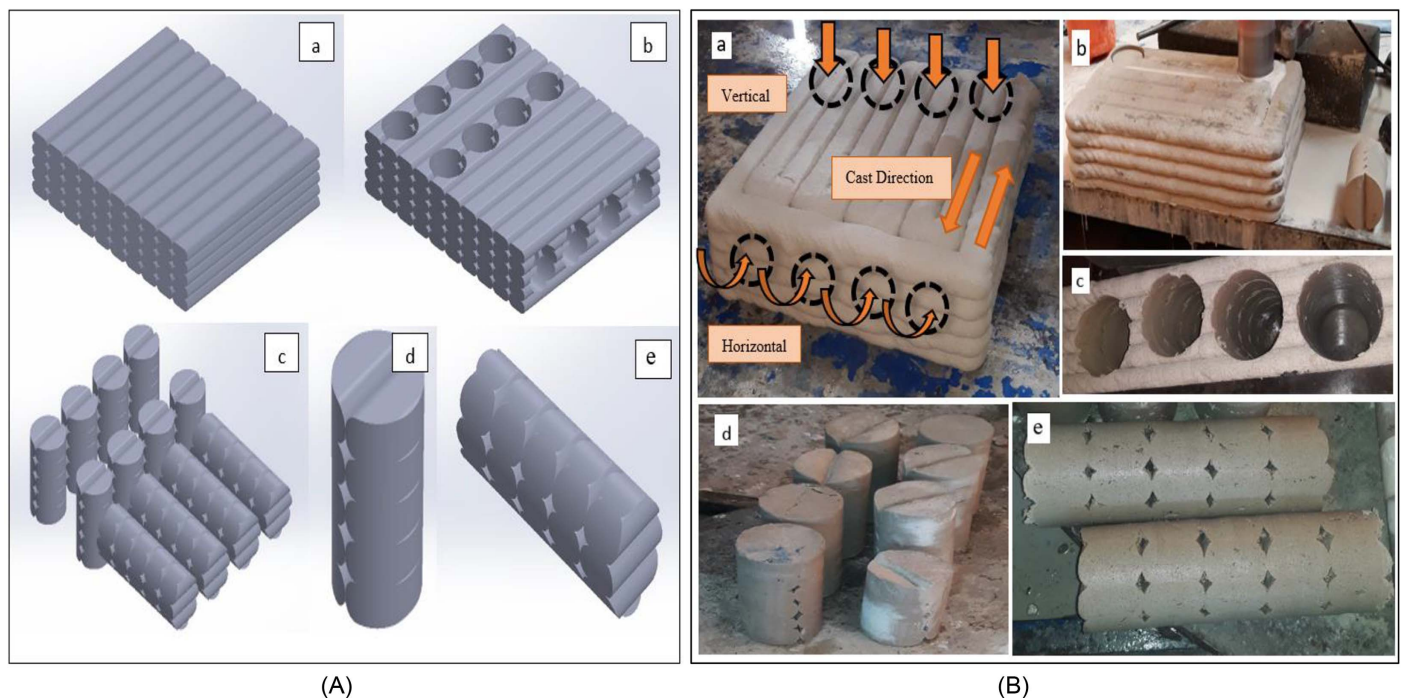


Fig. 2. Samples designed in SOLIDWORKS before 3D printing and their produced counterparts after 3D printing. (A) schematic representation of core samples [(a) perspective view; (b) remaining part after core drilling; (c) vertical and horizontal cores of a group; (d) vertical core; and (e) horizontal core]; and (B) actual images of core samples [(a) 3D printed concrete slab; (b) vertical coring process; (c) shape of after-drilled horizontal cores; (d) vertical cores; and (e) horizontal cores].

The tests for water absorption via capillary rise were carried out based on TS EN 13057 (TS 2004) on samples that were dried in a ventilated oven at $(40^{\circ}\text{C} \pm 2^{\circ}\text{C})$ for seven days until reaching a constant mass. The capillary absorption test consisted of immersing the cores 2 ± 1 mm in water and regularly weighing mass increases after 12 min, 30 min, 1 h, 2 h, 4 h, and 24 h immersed in water. The water level was kept constant during testing by checking the immersion depth. The sorptivity coefficient, k ($\text{cm} \cdot \text{s}^{-1/2}$), was obtained using Eq. (1)

$$Q/A = k\sqrt{t} \quad (1)$$

where Q = amount of water absorbed (cm^3); A = cross section of the core in contact with water (cm^2); and t = time (s). From the Q/A plot against the square root of time, k was calculated from the slope of the linear relationship between two variables.

Microstructural analyses were also performed by mercury intrusion porosimetry (MIP), gas absorption by the Brunauer-Emmett-Teller (BET) technique, and scanning electron microscopy (SEM).

A mercury porosimeter operates on the principle that an inert, non-wetting liquid, at a contact angle greater than 90° , cannot enter tiny pores unless adequate pressure is applied. The Washburn equation delivers the relationship between applied pressure and pore diameter as

$$D = (-4\gamma \cos \theta)/P \quad (2)$$

where P = applied pressure; γ = surface tension of the mercury (480 dyne/cm); θ = contact angle between the mercury and the pore wall (usually 140°); and D = pore diameter. MIP tests were performed on a Quantachrome Corporation, Poremaster 60 mercury porosimeter with a pressure of 55,000 psi. MIP analysis was carried out on samples with a diameter of approximately 7 mm, obtained by breaking 3D cores, which were kept in the laboratory environment for 180 days. Samples were dried at about 105°C before testing.

For BET analysis, 180-day old samples were ground to powder and dried at 105°C . The analysis was performed with a Micromeritic 3Flex Version 5.00 Surface Characterization Device. MicroActive Data Reduction software was used for the BET analysis.

SEM samples were obtained from the inner parts of concrete elements to reduce carbonation effects from the surface as much as possible. SEM analysis was performed on approximately 7–10 mm diameter sections taken from the 335-day-old 3D concrete core samples. Samples were smoothed in a stone cutting machine, and the surface to be examined was prepared by applying very thin (approx. 3 Å/s) gold plating under a vacuum. Analyses were carried out with

an SEM with an EDX connection (Zeiss Sigma 300, Germany) using a System Schottky Field-Emission electron gun and a 4-segment backscatter electron detector (BSD).

Results and Discussion

Evaluation of Results of the Unit Weight Test

Accordingly, the unit weights of the A0, A1, A1.5, and A2 groups were 2,130, 1,820, 1,780, and 1,670 kg/m^3 , respectively. As seen from the data, the unit weights decreased as the AEA dosage in the mixtures increased. The densities of all groups, except the group without air entrainment (A0), were within the lightweight concrete class densities according to ACI Committee 213: Guide for Structural Lightweight Aggregate Concrete (2003). Extra evaluations of the unit weights of fresh 3D concrete mixtures are given in Tarhan and Şahin (2021).

As stated in the Materials section, a cocktail of chemical additives was considered to achieve the desired 3D concrete rheology. Some of the admixtures, such as superplasticizers and viscosity modifiers, are surfactants that can reduce the surface tension of water in concrete (Faroug et al. 1999; Mardani and Emin 2023). It was evaluated that air bubbles in concrete mixes may have increased with the synergistic effect of multiple admixtures, and the stability of these entrained-air bubbles may have been preserved with the addition of viscosity modifying agent (VMAs). As a matter of fact, some researchers [Assad et al. (2003) and Zhang et al. (2020)] have noted that VMAs can reduce the surface energy of surfactant molecules and strengthen the liquid film, thus supporting the persistence of entrained-air bubbles and the homogeneity of air voids.

The unit weight of the hardened specimens was evaluated on cores drilled from 3D-printed concretes. Experimental results of unit weight tests of the 3D concrete in the fresh and hardened states are shown together in Fig. 3. The graph also shows the average unit weights of hardened 3D concretes. Since the curing process and coring was carried out on hardened concrete, the unit weight of fresh 3D concrete was shown for only four different mixtures (A0, A1, A1.5, and A2).

The unit weights of both fresh and hardened 3D concrete decrease as the ratio of AEA in the mix increases. It was found that compared to mixtures without AEA, the unit weights of fresh 3D concrete containing 0.1%, 0.15%, and 0.2% AEA decreased by 14.5%, 16.4%, and 21.6%, respectively, while the unit weights of hardened 3D concrete decreased by 4.4%, 15.3%, and 14.8%, respectively. These results indicate that the reduction in the unit weight

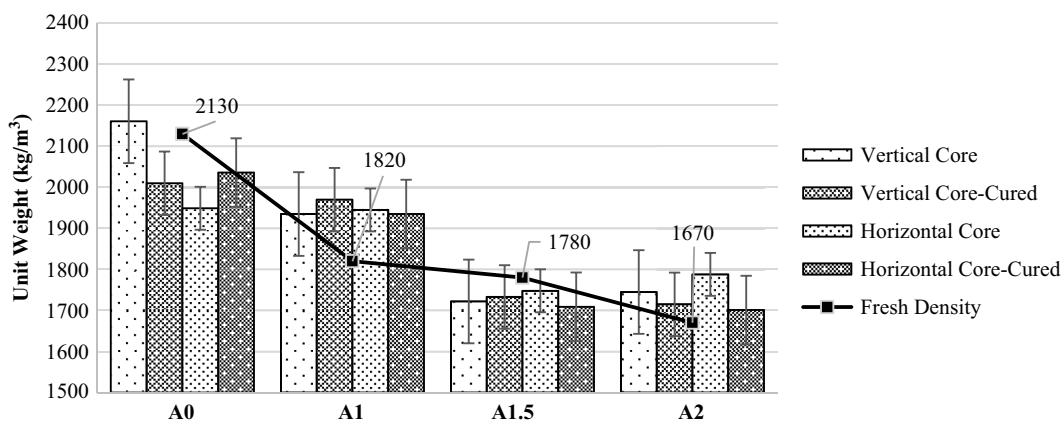


Fig. 3. Unit weights of 3D-printed concrete in the fresh and hardened state (kg/m^3).

of fresh 3D concrete is higher than that of hardened 3D concrete. This means that as the dosage of AEA increases, the unit weight of the fresh 3D concrete decreases more than that of the hardened 3D concrete. One possible explanation for this difference is that some of the AEA-induced air voids, which occupy voids and reduce the density of the fresh concrete, are lost during the 3D printing process. These air voids may be lost through a variety of mechanisms, such as compaction or displacement as the layers of concrete are deposited.

Although the lowest unit weight value belongs to the A1.5 group, the unit weights of A1.5 and A2 groups are close to each other and considerably lower than those of the A0 and A1 groups. According to Fig. 3, the unit weight of the vertical cores is significantly higher than the horizontal cores in groups A0 and A1, while this difference is not significant in groups A1.5 and A2. The unit weights of the horizontal and vertical cores are almost the same in the A1.5 and A2 groups. Since the air content is lower in groups A0 and A1 than in groups A1.5 and A2, the layers may have collapsed slightly during the 3D printing process due to the layers being more densely packed due to the concrete's weight and the overlying layers' compression effect, so cores taken perpendicular to the printing direction may be slightly heavier. In groups A1.5 and A2, possible defects in the samples were minimized due to the good printability resulting from the effect of air entrainment, and the layers are also light, so no collapse occurred, causing the anisotropic effect to disappear.

Evaluation of Results of the Capillary Water Absorption Tests

Capillary water absorption tests were performed when the cores taken from the 3D concrete were 56 days old. The sorptivity coefficients of the cores are given in Fig. 4.

From the graph in Fig. 4, it is seen that the water absorption coefficients of the samples increased as the dosage of AEA in the concrete increased. It was evaluated that the increase in the dosage of AEA might have led to an increase in the total volume of capillary pores in the concrete.

The average sorptivity coefficients for the A0, A1, A1.5, and A2 groups were 51.1, 65.3, 87.8, and 84.7 ($\text{g}/\text{cm}^2 \cdot \text{s}^{0.5} \times 10^{-5}$), respectively. As can be seen from these values, the group with the highest water absorption coefficient is the A1.5 group, not the A2 group, although the difference is small. These results suggest that based on the 3D concrete samples produced in this study, capillary water absorption increased with the addition of AEA, but there appeared to be an upper limit to this increase.

The effectiveness of an AEA in reducing surface tension in concrete is dependent on its concentration, which is often limited by a critical micelle concentration (CMC). The CMC is the maximum concentration of the surfactant before micelles begin to form, beyond which there is no further reduction in surface tension. If the AEA concentration is below the CMC, it will migrate to the water-air interface and lower the surface tension, with some molecules remaining dispersed within the bulk. However, if the AEA concentration exceeds the CMC, excessive amounts of AEA will form micelles, and only a limited amount of added surfactants will enter the dispersed phase or migrate to the water-air interface (Souza et al. 2017). For this study, the CMC value of AEA was found to be 0.15%. This was confirmed in nearly all tests, including capillary water absorption, compressive strength, and UPV.

According to the graph in Fig. 4, the capillary water absorption coefficients of the vertical samples are generally higher than the horizontal samples. Specifically, the average capillary water absorption coefficient for the vertical samples is $78.41 (\text{g}/\text{cm}^2 \cdot \text{s}^{0.5} \times 10^{-5})$, while the average for the horizontal samples is $66.08 (\text{g}/\text{cm}^2 \cdot \text{s}^{0.5} \times 10^{-5})$. This suggests that the orientation of the core samples can affect their capillary water absorption coefficients.

It is also noted that the unit weight of the vertical samples is $1,874.1 \text{ kg}/\text{m}^3$, while the unit volume weight of the horizontal samples is $1,851.4 \text{ kg}/\text{m}^3$. So, the larger unit volume weights of the vertical samples indicate that they have fewer micro and macro voids, which means that they are denser and have a greater surface area to hold water. As a result, more water was absorbed by the capillarity effect in the vertical samples, leading to a higher average capillary water absorption coefficient compared to the horizontal samples. According to the capillary water absorption test results, the lowest anisotropic effect was observed in the A1 group. High anisotropic differences were observed in the A0 and A1.5 groups, while low anisotropic differences were observed in the A2 group. The significant difference in capillary water absorption between the vertical and horizontal samples in the A0 group, where no AEA effect was observed, proves that the 3D printing process of this group of samples is different from the other groups. Therefore, it can be said that AEA directly affects the 3D printing process by affecting the cavity structures of the samples and increasing the print quality. The high anisotropic effects in the A1.5 group are explained as follows: since this group of samples contains a very high amount of AEA, the layers are very light (as seen from the unit volume weight results), so the layers continued to connect with each other, maintaining the voids both in the inside layer and between the layers.

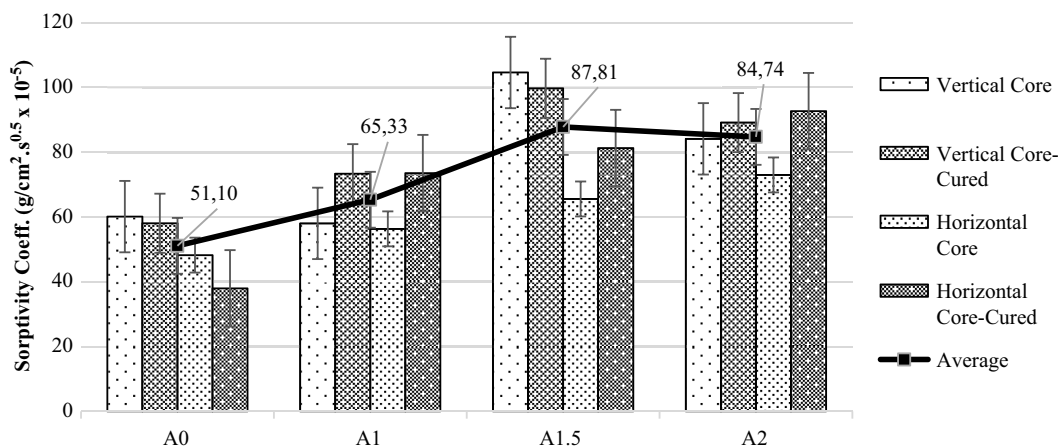


Fig. 4. Water absorption coefficients of all mixtures.

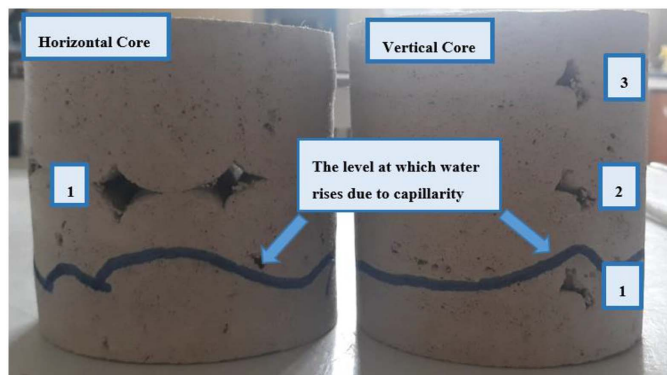


Fig. 5. The water heights formed in the core samples at the end of 24 h in the capillary water absorption test.

The A2 group had many more air voids and, therefore, the lightest layers. As can be seen from the SEM analysis results, this group of samples has a very large amount of voids, both micro and macro, so the anisotropic effect was not felt. This is due to the fact that all specimens retained the presence of voids within or between the layers, which are very well placed due to the high workability provided by the AEA.

Since the pore structure between the layers of the cores taken in the vertical is quite different from the horizontal ones (see Fig. 5), the increase of water by capillarity in the horizontal cores was higher than in the vertical cores. As seen in Fig. 5, there are three large gaps between the filaments in the cores taken vertically, but there is one large gap in the horizontal ones. It was decided that these gaps between the filaments prevent the capillary rising of water while the water continues to rise in the areas where there is contact between the filaments.

At the end of 24 h, the water, which was expected to rise to the summit points due to capillarity at the layer joints, could only rise a few centimeters in the 3D core samples. As another factor preventing the water from rising through the capillaries, in this study, it was thought that the capillary void ratio decreased due to the transformation of the voids in the concrete into circular and independent shapes due to the effect of the AEA. Even in the air-entrainment-free concrete produced in this study, due to the high number of chemicals used, water could only rise to the level of the first large gap between the layers after 24 h due to the capillarity effect.

Another aim of this study is to investigate the concrete curing compounds on 3D concrete engineering properties. The average capillary water absorption coefficient of the cured samples is 75.73, and the capillary water absorption coefficient of the uncured samples is $68.76 \text{ (g/cm}^2 \cdot \text{s}^{0.5} \times 10^{-5})$. In addition, the unit weight of the uncured samples is $1,874.2 \text{ kg/m}^3$ on average, while the unit volume weight of the cured samples is $1,851.2 \text{ kg/m}^3$. As can be seen from these data, the results are consistent with each other. However, it was found to be interesting that the capillary effect is more pronounced in the cured samples. This result does not necessarily indicate that the use of these concrete curing compounds positively affected the capillarity of this 3D concrete because high levels of capillary water absorption can be detrimental to the durability of concrete, as it can lead to the ingress of water into the pores of the concrete and increase the risk of freeze-thaw damage and other forms of deterioration.

Capillary water absorption coefficients were measured in this study according to TS EN 13057 (TS 2004). This standard is for traditional concrete, but the 3D concrete void system differs from conventional. So the water levels did not rise to the expected height due to large size gaps between the layers. At the end of the 24 h in which the samples came into contact with water, the water only rose about 3–4 cm in almost all of the samples. The capillary water absorption test gives information about the material's permeability (mortar) since it is an experiment that measures water's capillary rise. In 3D concretes, the structure consists of different layers and large (non-capillary) gaps between the layers. Therefore, the validity of this classic capillary water absorption test developed for conventional concrete samples should be discussed for 3D-printed concrete samples.

Evaluation of Ultrasonic Pulse Velocity (UPV) Tests Results

The results of the UPV testing are shown in Fig. 6.

As can be seen from Fig. 6, the UPV values of the cores decreased as the proportion of AEA added to the mixes increased in the A0, A1, and A1.5 groups, but in the A2 group, the UPV increased again. Average UPV values (vertical, horizontal, cured, and uncured) of the A0, A1, A1.5, and A2 groups were 3,843, 3,786, 3,267, and 3,324 m/s, respectively. UPV values obtained from the A0 and A1 groups were significantly higher than those of the A1.5 and A2 groups. The curing process did not significantly contribute to the UPV results of the concrete cores. As can be seen, the UPV results

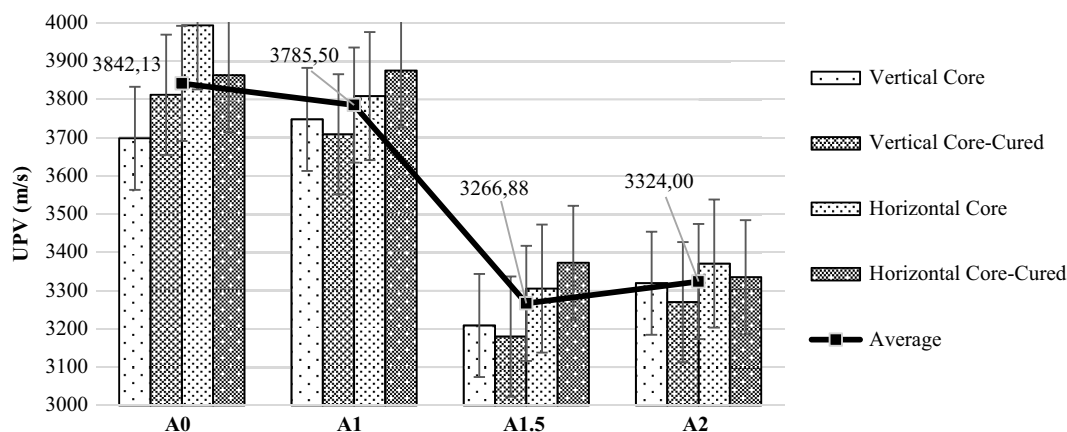


Fig. 6. UPV test results of all 3D-printed concrete cores.

of the cured specimens are almost equal to the uncured specimens for the same group.

In this study, the UPV of 3D concrete was found to be higher in cores taken in the horizontal direction compared to those taken in the vertical direction. This difference was attributed to the presence of one gap between layers in horizontal cores, compared to three gaps in vertical cores. 3D concrete is characterized by a layered structure created through the additive manufacturing process, which can lead to mechanical anisotropy. During ultrasonic sound transmission in 3D concrete, sound waves are transmitted from one probe to the other through the regions of interlayer adherence. However, in 3D concrete, the presence of interlayer gaps can obstruct the transmission of sound waves, leading to longer transmission times compared to conventional concrete. These findings suggest that the presence of gaps between layers in 3D concrete can impact its ultrasonic properties, and further research could help to understand this phenomenon better.

Evaluation of Compressive Strength Test Results

A graph of compressive strength test results applied to the 28-day 3D concrete cores is given in Fig. 7.

The compressive strength data presented in Fig. 7 clearly indicates significant differences between the four groups tested. The average values of groups A0 and A1 exhibit similar compressive strength values of 24.8 and 29.1 MPa, respectively, indicating that these groups have similar levels of strength. However, the compressive strength values of A1.5 and A2 are much lower than those of A0 and A1, with values of 15.2 and 15.7 MPa, respectively. Additionally, A1.5 and A2 have similar compressive strength values and are both considerably weaker than A0 and A1. Interestingly, the fact that A1.5 and A2 groups have similar compressive strengths indicates that adding AEA past the CMC value no longer significantly affects the compressive strength. The compressive strength of the 3D concrete samples showed a nonlinear decreasing trend as AEA increased in the mixes. It is observed that AEA decreases the compressive strength of concrete, and this rate varies according to the proportion of AEA in the mix.

The main reason for the close compressive strength values of the A0 and A1 groups is thought to be the increased workability properties of 3D concrete mixtures due to the addition of AEA. This, in turn, increases the bond strength between the filaments, leading to an increase in strength. Therefore, the use of AEA at minimum dosages actually increased the strength instead of decreasing it,

contrary to expectations. However, if more than 0.1% AEA was used, it resulted in reducing the strength by almost half.

It was stated in the study of Tarhan and Şahin (2021), which was published as the first step of this study and included the results of fresh concrete experiments, that the compressive strengths of $5 \times 5 \times 5$ cm³ samples produced by the casting method were 54.5, 28.6, 18.9, and 11.75 MPa for the A0, A1, A1.5, and A2 groups, respectively. Compared to the averages given above, without considering the size and shape effect of the test samples, there was a strength loss of 50% when the A0 mixture was generated by 3D production. So it can be said that the compressive strength results were quite different in conventional and 3D production without the AEA effect. But when it came to AEA's effect, the situation was different. For example, nearly the same values were obtained when producing without 3D-printed concrete (28.6 MPa) and the 3D technique (29.1 MPa) in the A1 group, while a 20% decrease in strength was observed for 3D production in the A1.5 group. In the A2 group, contrary to the other sets, there was a 33% increase in compressive strength for the 3D production method.

As shown in Fig. 7, the compressive strength of vertical cores was higher than those of horizontal cores in all groups. Since the cores taken in the vertical direction were perpendicular to the printing direction (i.e., to the lamination), the compressive strengths of the 3D concrete were higher than those of the samples taken from the layers parallel to the casting (see Fig. 2). The bonds in the horizontal direction were weaker than the applied forces, and the samples separated easily.

Normally, compressive strength and UPV results in conventional concrete are expected to be compatible. However, this is not meaningful for 3D concretes. As can be seen from the results of this study, the compressive strength of the samples taken perpendicular to the casting direction was expected to be high, and the results confirmed this. However, for the UPV results, the number of voids between the layers was a more effective parameter than the layers' casting direction. The relationship between UPV results and the compressive strength tests is shown in Fig. 8.

As seen in Fig. 8, the relationship between compressive strength and UPV is not compatible in any of the groups. Except for the A1 group, the effect of the curing compound on the cores' compressive strength was positive. In the A0 group, the average compressive strength of uncured specimens was 22.8 MPa, while those of the cured ones were 31.5 MPa. However, the compressive test results of the other groups were quite close to each other. Comparison of UPV and compressive strength results under the effect of curing

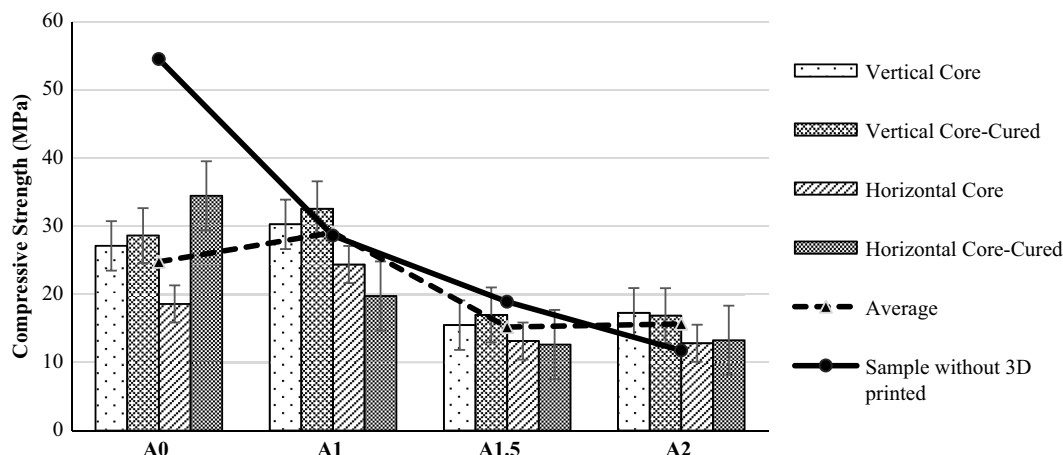


Fig. 7. Compressive strengths of the samples according to the AEA.

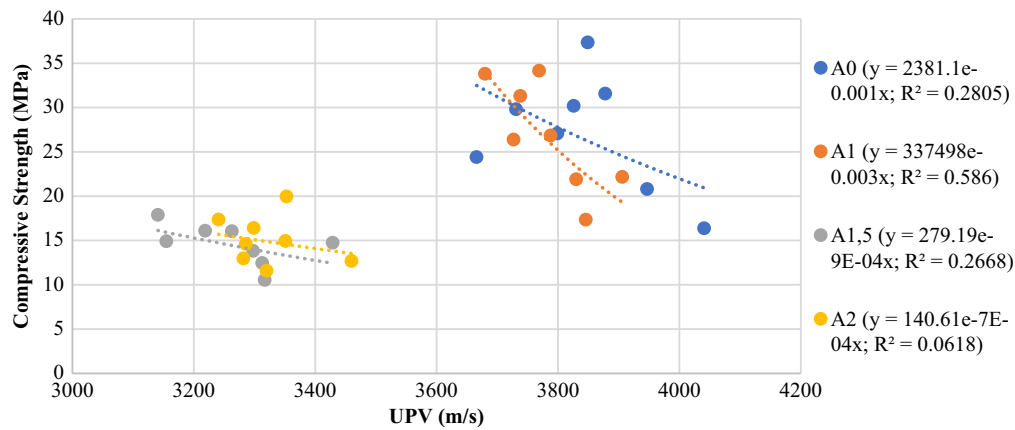


Fig. 8. Relationship between UPV and compressive strength test results in terms of AEA rates.

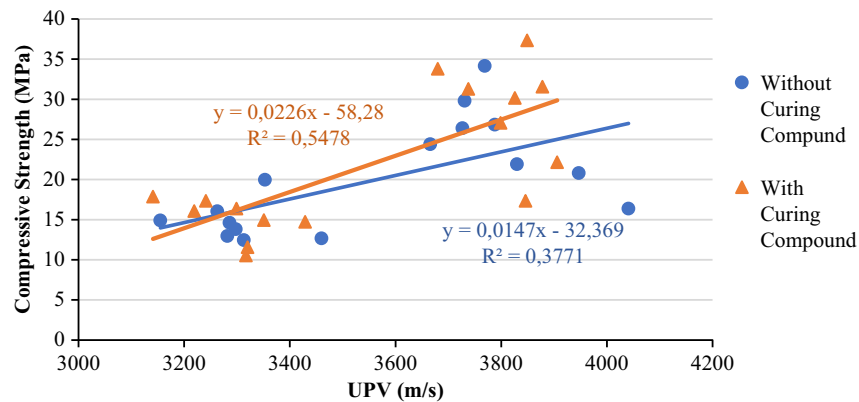


Fig. 9. Relationship between UPV and compressive strength test results in terms of samples with and without curing compound.

additive is again not significant, as seen in Fig. 9. While the effect of the curing compound was not obvious in the UPV test results, it affected the compressive strength results.

The finding here that the compressive strength of 3D-printable concrete varies with the orientation of the layers confirms results from other researchers. In addition to the effect of the entrapped and entrained-air void system, gaps and cold joints formed naturally in 3D concrete during manufacturing are also crucial parameters for the compressive strength of the concrete.

Evaluation of the Micropores of the Samples Based on BET and MIP Test Results

By obtaining isothermal curves with BET analysis, mesopores and micropores in the samples were determined. In addition, some properties, such as pore size distribution graphs, average void diameter, and surface area of the samples, were determined. Table 1 shows the microstructural properties obtained from the samples by BET analysis.

Pore size distributions of the samples are given in Fig. 10. Since the samples taken for BET analysis were very small, it does not matter whether they were taken from the horizontal or vertical samples. Only curing additive and air-entraining effect were investigated.

A detailed assessment of the pore size distribution of the samples, including the mean pore diameter and surface area, was obtained from the BET analysis in Tarhan (2020). As seen in Fig. 10, the pore size distributions of all groups varied between 2 and 170 nm. The

Table 1. Microstructural features determined by BET analysis

Sample name	BET surface area	BJH		Adsorption average pore diameter (nm)	Desorption average pore diameter (nm)
		adsorption cumulative volume of pores (cm ³ /g)	desorption cumulative volume of pores (cm ³ /g)		
A0	19.4933	0.038621	0.039358	4.9607	6.0587
A0K	2.6650	0.022090	0.022048	16.6973	23.1739
A1	3.3750	0.017479	0.017622	9.4069	12.2713
A1K	1.8407	0.024564	0.024442	17.9153	26.2652
A1,5	3.1153	0.026797	0.026777	12.6163	18.0018
A1,5K	3.3714	0.026731	0.026752	12.2970	16.5445
A2	3.1099	0.026389	0.026434	10.5237	16.2666
A2K	5.8443	0.034241	0.034574	8.4810	11.1188

AEA-free and uncured group (A0) had a higher volume of cylindrical pores with radii in the 2–14 nm range, followed by the A2K with a volume of cylindrical voids with radii in the range of 2–8 nm. The volume of cylindrical pores of the other groups was not concentrated in a specific range, and the radii of the pores changed homogeneously between 2 and 170 nm. The highest peak around 2 nm was obtained in the A0 sample, and most of the voids of the sample were around this value. Therefore, as expected, the smallest pore size distribution is in this sample. In the other groups,

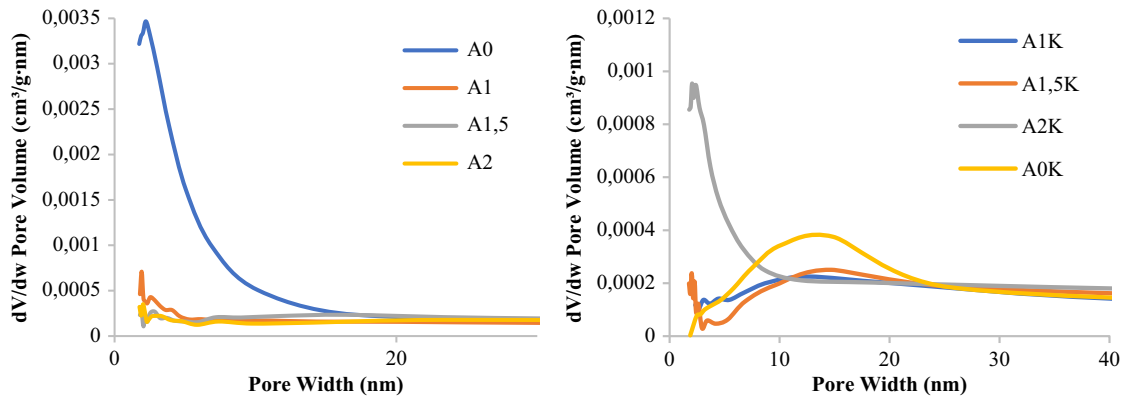


Fig. 10. The pore size distribution of samples determined by the BET technique.

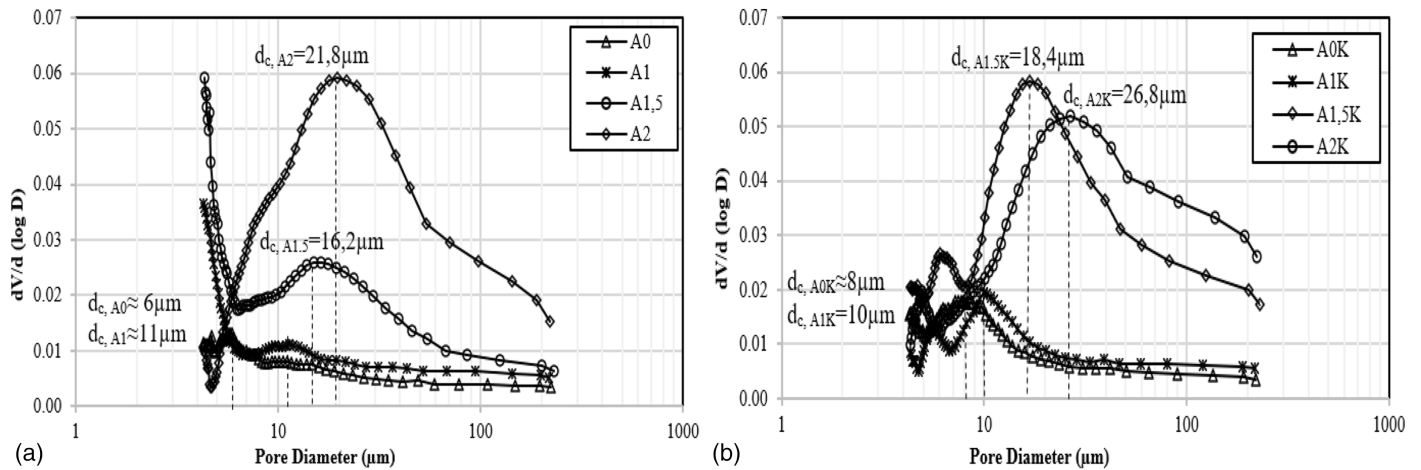


Fig. 11. Differential curves were measured by an intrusion procedure of the groups with (a) AEA; and (b) cured (The D and V values on the y-axis represent the diameter of the inlet pore size and volume of the pores with diameter D, respectively).

in parallel with the air-entraining additive ratio, the void sizes of the samples increased, and their distribution became homogeneous.

In this study, the MIP test, a widely used technique to characterize the distribution of pore sizes in cementitious material, was also performed to identify macropores in the samples. Differential curves and critical pore diameters (d_c) obtained from MIP are given in Fig. 11.

The MIP analysis determined pore sizes ranging from approximately 5 to 250 μm for all group samples. As seen in Figs. 11(a and b), adding AEA to the mixtures changes the pore size distribution of 3D-printed mortars, and the number of pores in the samples increases with the amount of AEA in the mixes. For both categories, the finest groups were A0 and A1, while the number of voids and void diameters were larger in the A1.5 and A2 groups. According to this, it can be said that the increase in the amount of AEA, even at very low rates, causes a large increase in both the void diameters and the void amounts of the sample. On the other hand, for both categories, the pore size distributions of the A0 and A1 groups were similar, while those of the A1.5 and A2 groups were similar.

Gradation of the critical pore diameters of the groups according to their AEA ratio and curing process was calculated as follows

$$d_{c,A2} > d_{c,A1.5} > d_{c,A1} > d_{c,A0} \quad (3)$$

$$d_{c,A2K} > d_{c,A1.5K} > d_{c,A1K} > d_{c,A0K} \quad (4)$$

As can be seen from the inequalities in numbers (3) and (4), the critical void diameters of the mixtures increased with the addition of AEA to the mixes. The average critical pore diameters of both groups were close to each other ($d_{c,ort} = 14 \mu\text{m}$ for mixes with AEA and $d_{c,ort} = 16 \mu\text{m}$ for cured mixtures).

The critical pore diameter controls permeability, and the larger the critical pore size, the worse the impermeability of cement-based materials. In the section “Evaluation of Results of the Capillary Water Absorption Tests,” it was stated that the capillarity coefficients of the material increased with the addition of AEA to the mixtures. When this result was considered together with the above findings, the relationship between critical pore diameter and permeability of the samples was confirmed.

Microstructural Evaluations Based on SEM Observations

SEM analysis was performed to visualize the change in voids in the microstructure with the AEA. The SEM images are presented in Fig. 12.

It can be seen from Fig. 12 that all samples, including the A0 group, have entrained-air pores. As stated in Tarhan and Şahin (2021),

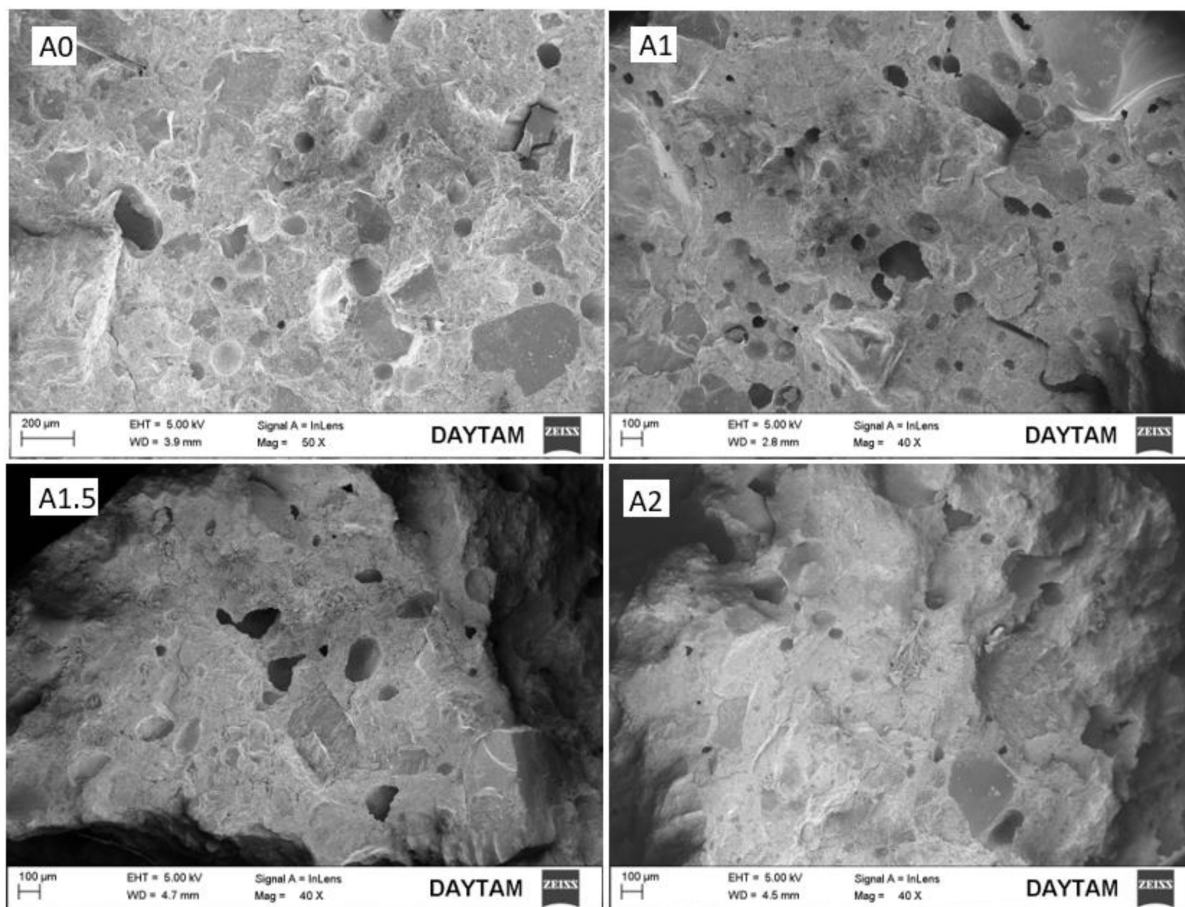


Fig. 12. SEM images displaying pores of the samples with four compositions.

the group without AEA (A0) showed spherical and independent air spaces due to the large number of chemical additives used during production. As seen in Fig. 12, the air pores in the A0 and A1 groups were more spherical and generally homogeneously distributed in the sample. However, the pore diameters in the A1.5 and A2 groups increased, and air pore shapes and distribution in the sample became irregular. Due to this irregular internal structure of the A1.5 and A2 groups, the strength and durability properties were found to be weak. Therefore, all the results obtained within the scope of this study corroborated with one another.

As additional information, SEM images showing cement hydration products, fibers, aggregates, and the internal structure of the pores of the samples are given in Fig. 13. Similar crystal forms and structures were observed in all groups. SEM images taken from the A1 group were shown in the figure as an example.

As seen in Fig. 13, ettringite crystals formed 3D concretes. In addition, one of the solid concrete components (aggregate) and the fibers added to the mixtures during production are displayed.

Ettringite ($3\text{CaO} \cdot \text{Al}_2\text{O}_3 \cdot 3\text{CaSO}_4 \cdot 32\text{H}_2\text{O}$) crystals formed on the walls of an air pore are shown in Figs. 13(a and b). These crystals were observed in entrained-air pores and in some cracks. Since the cement dosage of the 3D concrete produced within the scope of this study was high (680 kg/m^3), it was expected that the formation of ettringite would be high. For example, a pore in the SEM micrograph given in Fig. 14 was found to be filled with ettringite crystals, and in the EDX analysis performed on this area, it was determined that there was sulfate in the pore.

Conclusions

In this study, the effects of AEA on the physicochemical properties of 3D concrete were investigated using hardened concrete tests. The parameters used in the study were AEA ratio, curing compound application status, and core orientation. Since the imperfect structure between the layers causes 3D concretes to exhibit anisotropic material properties, all the investigated properties varied depending on the direction.

The sorptivity coefficients of cores taken in the vertical direction were higher than those in the horizontal samples, but the accuracy of the water absorption tests was questionable due to the influence of large gaps in the samples. Therefore, the development of a new experimental method to determine the water absorption of 3D concrete has been proposed. The compressive strength of 3D-printed concrete decreased with increased AEA in the mixes, and the compressive strength of vertical cores was generally higher than those of horizontal cores. The traditional uniaxial compression test was found to be unsuitable for 3D-printed concrete due to its anisotropic character, and it is recommended to determine the compressive strength of 3D concrete using a triaxial compressive strength test instead. Applying the membrane-forming curing compound to 3D concrete elements is very practical in terms of use and is a very useful method for curing 3D elements.

The BET and MIP tests technique revealed that the diameters of the macro- and micropores of the mixtures increased with the addition of AEA to the mixes. Also, SEM images showed that adding

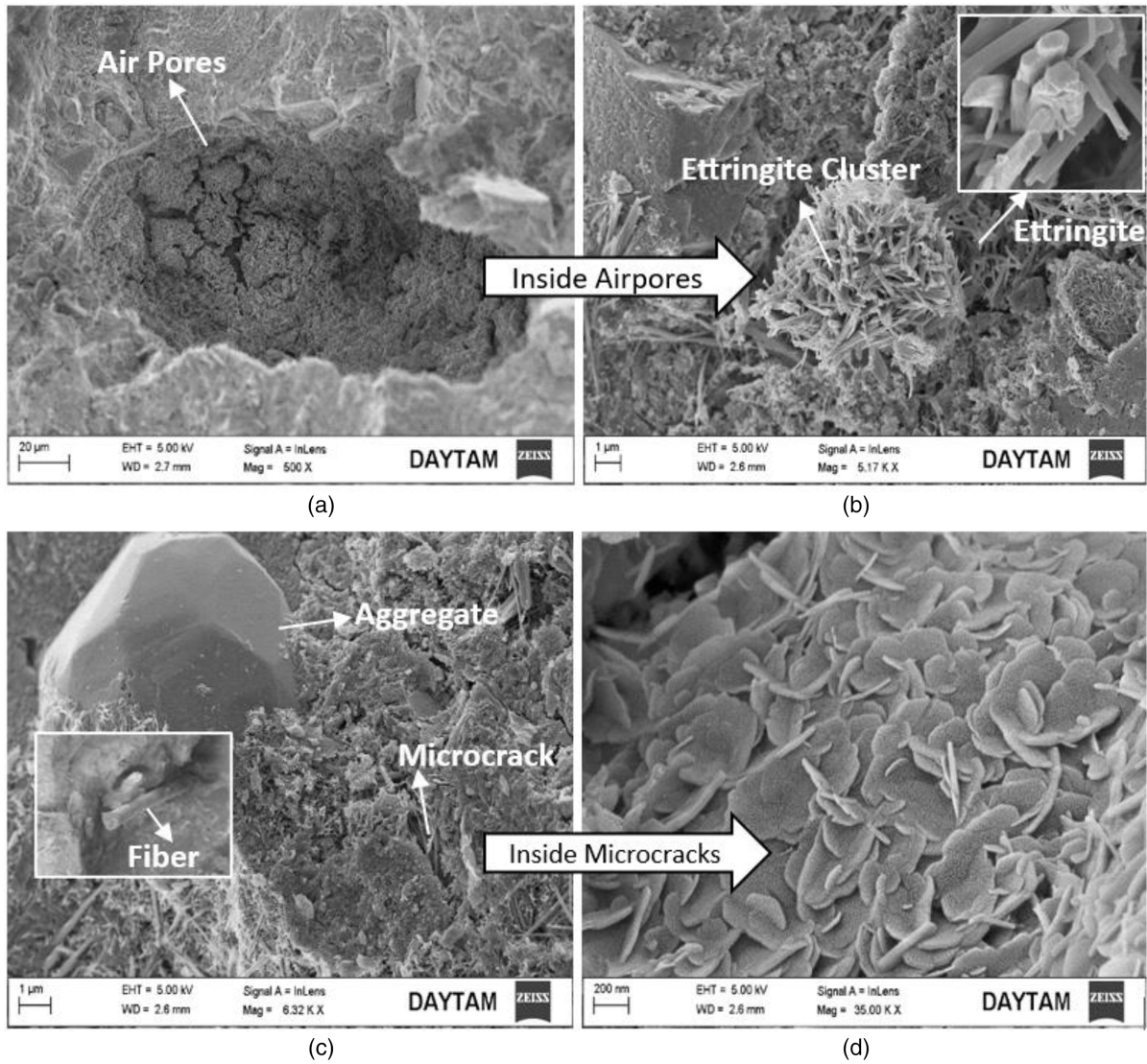


Fig. 13. SEM images were obtained from the A1 group: (a) a view of air pores; (b) ettringite formation inside the air pores and close-up view of the ettringites; (c) aggregate, fiber, and cement paste with microcracks of the sample; and (d) close-up view of microcracks.

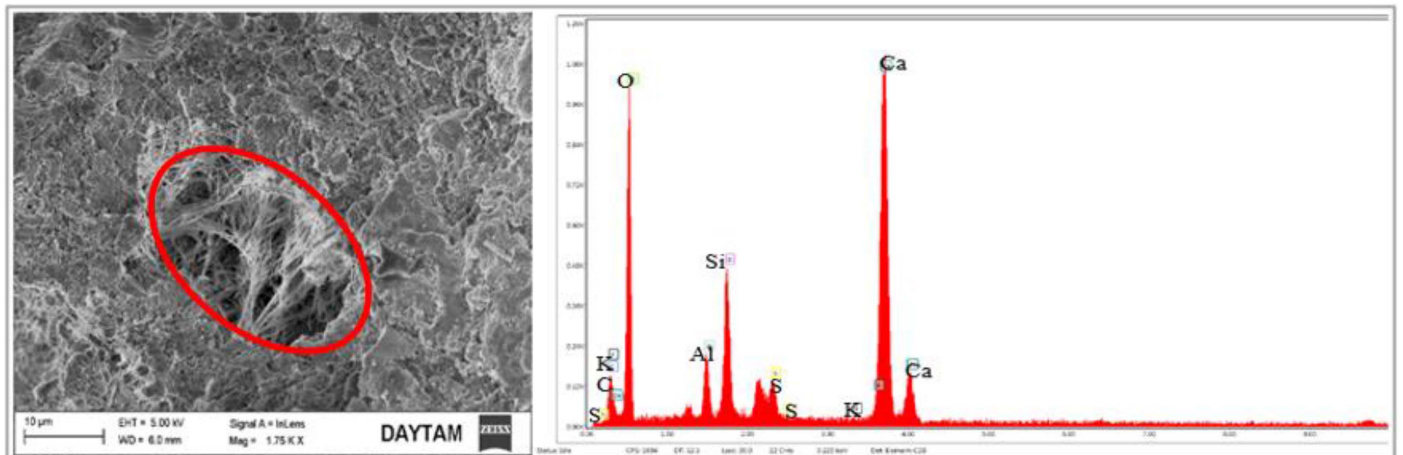


Fig. 14. Ettringite in air pores and EDX analysis in this area.

AEA to fresh 3D concrete forms numerous small, spherical, and discrete voids within the cement paste.

The layering of 3D concrete led to differences in the physico-mechanical properties of cores taken from the same element in the vertical and horizontal directions. These differences were caused by the layer structure itself and defects between the layers, resulting in anisotropic behavior in 3D concrete. The addition of high levels of AEA to 3D concrete increased the pore volume and negatively affected the physico-mechanical properties of the specimens. However, the addition of low levels of AEA (the optimum amount in this study was 0.1%) improved the workability of 3D concrete mixtures and resulted in more seamless 3D elements. This, in turn, positively affected hardened concrete properties, including compressive strength, although a decrease in mechanical properties was expected due to the AEA effect. In other words, incorporating low amounts of AEA improved the workability of 3D concrete and even provided anisotropic benefits by reducing the effect of weaknesses between layers. Future studies should focus on defining the optimal air content and analyzing other key parameters of air entrainment in 3D concrete (such as specific surface, void factor, and void frequency). Furthermore, computed tomography (CT) slices can be used to validate the results from a mesoscale perspective.

Data Availability Statement

Some or all data, models, or code that support the findings of this study are available from the corresponding author upon reasonable request.

References

- ACI (American Concrete Institute). 2003. *Guide for structural lightweight aggregate concrete*. ACI 213. Farmington Hills, MI: ACI.
- Arunothayan, A. R., B. Nematollahi, R. Ranade, K. H. Khayat, and J. G. Sanjayan. 2021. "Digital fabrication of eco-friendly ultra-high performance fiber-reinforced concrete." *Cem. Concr. Compos.* 125 (Jan): 104281. <https://doi.org/10.1016/j.cemconcomp.2021.104281>.
- Assaad, J., K. H. Khayat, and H. Mesbah. 2003. "Assessment of thixotropy of flowable and self-consolidating concrete." *ACI Mater. J.* 100 (2): 99–107. <https://doi.org/10.14359/12548>.
- Assaad, J. J., F. Hamzeh, and B. Hamad. 2020. "Qualitative assessment of interfacial bonding in 3D printing concrete exposed to frost attack." *Case Stud. Constr. Mater.* 13 (Dec): e00357. <https://doi.org/10.1016/j.cscm.2020.e00357>.
- Eugenin, C., I. Navarrete, W. Brevis, and M. Lopez. 2022. "Air bubbles as an admixture for printable concrete: A review of the rheological effect of entrained air." *3D Print. Addit. Manuf.* 9 (1): 64–80. <https://doi.org/10.1089/3dp.2020.0302>.
- Faroug, F., J. Szwabowski, and S. Wild. 1999. "Influence of superplasticizers on workability of concrete." *J. Mater. Civ. Eng.* 11 (2): 151–157. [https://doi.org/10.1061/\(ASCE\)0899-1561\(1999\)11:2\(151\)](https://doi.org/10.1061/(ASCE)0899-1561(1999)11:2(151)).
- Feng, P., X. Meng, J. F. Chen, and L. Ye. 2015. "Mechanical properties of structures 3D printed with cementitious powders." *Constr. Build. Mater.* 93 (Sep): 486–497. <https://doi.org/10.1016/j.conbuildmat.2015.05.132>.
- Hager, I., A. Golonka, and R. Putanowicz. 2016. "3D printing of buildings and building components as the future of sustainable construction?" *Procedia Eng.* 151 (Jan): 292–299. <https://doi.org/10.1016/j.proeng.2016.07.357>.
- Ingaglio, J., J. Fox, C. J. Naito, and P. Bocchini. 2019. "Material characteristics of binder jet 3D printed hydrated CSA cement with the addition of fine aggregates." *Constr. Build. Mater.* 206 (May): 494–503. <https://doi.org/10.1016/j.conbuildmat.2019.02.065>.
- Keita, E., H. Bessaies-Bey, W. Zuo, P. Belin, and N. Roussel. 2019. "Weak bond strength between successive layers in extrusion-based additive manufacturing: Measurement and physical origin." *Cem. Concr. Res.* 123 (Sep): 105787. <https://doi.org/10.1016/j.cemconres.2019.105787>.
- Kloft, H., H. W. Krauss, N. Hack, E. Herrmann, S. Neudecker, P. A. Varady, and D. Lowke. 2020. "Influence of process parameters on the interlayer bond strength of concrete elements additive manufactured by Shotcrete 3D printing (SC3DP)." *Cem. Concr. Res.* 134 (Aug): 106078. <https://doi.org/10.1016/j.cemconres.2020.106078>.
- Kruger, J., A. du Plessis, and G. van Zijl. 2021. "An investigation into the porosity of extrusion-based 3D printed concrete." *Addit. Manuf.* 37 (Jan): 101740. <https://doi.org/10.1016/j.addma.2020.101740>.
- Kruger, J., and G. van Zijl. 2021. "A compendious review on lack-of-fusion in digital concrete fabrication." *Addit. Manuf.* 37 (Jan): 101654. <https://doi.org/10.1016/j.addma.2020.101654>.
- Lu, B., M. Li, T. N. Wong, and S. Qian. 2021. "Effect of printing parameters on material distribution in spray-based 3D concrete printing (S-3DCP)." *Autom. Constr.* 124 (Apr): 103570. <https://doi.org/10.1016/j.autcon.2021.103570>.
- Lu, B., Y. Qian, M. Li, Y. Weng, K. F. Leong, M. J. Tan, and S. Qian. 2019. "Designing spray-based 3D printable cementitious materials with fly ash cenosphere and air entraining agent." *Constr. Build. Mater.* 211 (Jun): 1073–1084. <https://doi.org/10.1016/j.conbuildmat.2019.03.186>.
- Ma, G., Z. Li, L. Wang, F. Wang, and J. Sanjayan. 2019. "Mechanical anisotropy of aligned fiber reinforced composite for extrusion-based 3D printing." *Constr. Build. Mater.* 202 (Jun): 770–783. <https://doi.org/10.1016/j.conbuildmat.2019.01.008>.
- Marchon, D., S. Kawashima, H. Bessaies-Bey, S. Mantellato, and S. Ng. 2018. "Hydration and rheology control of concrete for digital fabrication: Potential admixtures and cement chemistry." *Cem. Concr. Res.* 112 (Oct): 96–110. <https://doi.org/10.1016/j.cemconres.2018.05.014>.
- Mardani, A., and A. Emin. 2023. "Utilization of high-range water reducing admixture having air-entraining agents in cementitious systems." *J. Build. Eng.* 64 (Apr): 105565. <https://doi.org/10.1016/j.job.2022.105565>.
- Moelich, G. M., J. Kruger, and R. Combrinck. 2021. "Modelling the inter-layer bond strength of 3D printed concrete with surface moisture." *Cem. Concr. Res.* 150 (Dec): 106559. <https://doi.org/10.1016/j.cemconres.2021.106559>.
- Nematollahi, B., M. Xia, J. Sanjayan, and P. Vijay. 2018. "Effect of type of fiber on inter-layer bond and flexural strengths of extrusion-based 3D printed geopolymer." *Mater. Sci. Forum* 939 (Mar): 155–162. <https://doi.org/10.4028/www.scientific.net/MSF.939.155>.
- Nerella, V. N., S. Hempel, and V. Mechtcherine. 2019. "Effects of layer-interface properties on mechanical performance of concrete elements produced by extrusion-based 3D-printing." *Constr. Build. Mater.* 205 (Apr): 586–601. <https://doi.org/10.1016/j.conbuildmat.2019.01.235>.
- Panda, B., J. H. Lim, and M. J. Tan. 2019. "Mechanical properties and deformation behavior of early age concrete in the context of digital construction." *Composites, Part B* 165 (May): 563–571. <https://doi.org/10.1016/j.compositesb.2019.02.040>.
- Panda, B., S. C. Paul, L. J. Hui, Y. W. D. Tay, and M. J. Tan. 2017. "Additive manufacturing of geopolymer for sustainable built environment." *J. Cleaner Prod.* 167 (Nov): 281–288. <https://doi.org/10.1016/j.jclepro.2017.08.165>.
- Paul, S. C., Y. W. D. Tay, B. Panda, and M. J. Tan. 2018. "Fresh and hardened properties of 3D printable cementitious materials for building and construction." *Arch. Civ. Mech. Eng.* 18 (Mar): 311–319. <https://doi.org/10.1016/j.acme.2017.02.008>.
- Şahin, R., M. A. Taşdemir, R. Gül, and C. Çelik. 2007. "Optimization study and damage evaluation in concrete mixtures exposed to slow freeze-thaw cycles." *J. Mater. Civ. Eng.* 19 (7): 609–615. [https://doi.org/10.1061/\(ASCE\)0899-1561\(2007\)19:7\(609\)](https://doi.org/10.1061/(ASCE)0899-1561(2007)19:7(609)).
- Sanjayan, J. G., B. Nematollahi, M. Xia, and T. Marchment. 2018. "Effect of surface moisture on inter-layer strength of 3D printed concrete." *Constr. Build. Mater.* 172 (May): 468–475. <https://doi.org/10.1016/j.conbuildmat.2018.03.232>.
- Soltan, D. G., and V. C. Li. 2018. "A self-reinforced cementitious composite for building-scale 3D printing." *Cem. Concr. Compos.* 90 (Jul): 1–13. <https://doi.org/10.1016/j.cemconcomp.2018.03.017>.
- Souza, M. T., C. K. Maykot, A. C. Z. Araújo, F. Raupp-Pereira, and A. N. de Oliveira. 2017. "Electrolytes' influence on foamability and

- foam stability of cement suspensions.” *Constr. Build. Mater.* 157 (Dec): 363–371. <https://doi.org/10.1016/j.conbuildmat.2017.09.043>.
- Tarhan, Y. 2020. “Investigation of freeze-thaw resistance and pore structure of digitally fabricated cement-based composites.” Ph.D. thesis, Institute of Science, Atatürk Univ.
- Tarhan, Y., and R. Şahin. 2019. “Developments of 3D concrete printing process.” In *Proc., Int. Civil Engineering and Architecture Conf.* Trabzon, Turkey: Golden Light Publishing.
- Tarhan, Y., and R. Şahin. 2021. “Fresh and rheological performances of air-entrained 3D printable mortars.” *Materials* 14 (9): 2409. <https://doi.org/10.3390/ma14092409>.
- Tay, Y. W. D., G. H. A. Ting, Y. Qian, B. Panda, L. He, and M. J. Tan. 2019. “Time gap effect on bond strength of 3D-printed concrete.” *Virtual Phys. Prototyping* 14 (1): 104–113. <https://doi.org/10.1080/17452759.2018.1500420>.
- TS (Turkish Standards). 2004. *Products and systems for the protection and repair of concrete structures—Test methods—Determination of resistance of capillary absorption*. TS EN 13057. Ankara, Turkey: TS.
- TS (Turkish Standards). 2019a. *Assessment of in-situ compressive strength in structures and precast concrete components*. TS EN 13791. Ankara, Turkey: TS.
- TS (Turkish Standards). 2019b. *Concrete—Hardened concrete tests—Part 3: Determination of compressive strength of test samples*. TS EN 12390-3. Ankara, Turkey: TS.
- TS (Turkish Standards). 2021. *Testing concrete in structures—Part 4: Determination of ultrasonic pulse velocity*. TS EN 12504-4. Ankara, Turkey: TS.
- Van Der Putten, J., M. Deprez, V. Cnudde, G. De Schutter, and K. Van Tittelboom. 2019. “Microstructural characterisation of 3D printed cementitious materials.” *Materials* 12 (18): 2993. <https://doi.org/10.3390/ma12182993>.
- Wolfs, R. 2015. “3D printing of concrete structures.” Graduation thesis, Dept. of the Built Environment Master Architecture, Building and Planning Specialization Structural Design, Eindhoven Univ. of Technology.
- Wolfs, R. J. M., F. P. Bos, and T. A. M. Salet. 2019. “Hardened properties of 3D printed concrete: The influence of process parameters on interlayer adhesion.” *Cem. Concr. Res.* 119 (May): 132–140. <https://doi.org/10.1016/j.cemconres.2019.02.017>.
- Wu, P., J. Wang, and X. Wang. 2016. “A critical review of the use of 3-D printing in the construction industry.” *Autom. Constr.* 68 (Aug): 21–31. <https://doi.org/10.1016/j.autcon.2016.04.005>.
- Xiao, J., Z. Chen, T. Ding, and S. Zou. 2022. “Bending behaviour of steel cable reinforced 3D printed concrete in the direction perpendicular to the interfaces.” *Cem. Concr. Compos.* 125 (Jan): 104313. <https://doi.org/10.1016/j.cemconcomp.2021.104313>.
- Zhang, J., X. Gao, and L. Yu. 2020. “Improvement of viscosity-modifying agents on air-void system of vibrated concrete.” *Constr. Build. Mater.* 239 (Apr): 117843. <https://doi.org/10.1016/j.conbuildmat.2019.117843>.
- Zhang, Y., Y. Zhang, W. She, L. Yang, G. Liu, and Y. Yang. 2019. “Rheological and harden properties of the high-thixotropy 3D printing concrete.” *Constr. Build. Mater.* 201 (Mar): 278–285. <https://doi.org/10.1016/j.conbuildmat.2018.12.061>.